The synapsin domain E accelerates the exo-endocytotic cycle of synaptic vesicles in cerebellar Purkinje cells

Anna Fassio[1], Daniela Merlo[1,*], Jonathan Mapelli[2], Andrea Menegon[3], Anna Corradi[1], Maurizio Mete[1], Simona Zappettini[1], Giambattista Bonanno[1,4], Flavia Valtorta[3], Egidio D'Angelo[2] and Fabio Benfenati[1,5,‡]

[1]Center of Neuroscience and Neuroengineering, Department of Experimental Medicine, University of Genoa, Italy
[2]Department of Cellular and Molecular Physiology and Pharmacology, University of Pavia, Italy
[3]San Raffaele Scientific Institute, 'Vita Salute' University and I.I.T. Unit of Molecular Neuroscience, Milan, Italy
[4]Center of Excellence for Biomedical Research, University of Genoa, Italy
[5]Unit of Neuroscience, The Italian Institute of Technology, Morego Central Laboratories, Genoa, Italy

*Present address: Department of Cell Biology and Neuroscience, Istituto Superiore di Sanità, Rome, Italy
‡Author for correspondence (e-mail: benfenat@unige.it)

Accepted 26 July 2006
Journal of Cell Science 119, 4257-4268 Published by The Company of Biologists 2006
doi:10.1242/jcs.03194

Summary

Synapsins are synaptic-vesicle-associated phosphoproteins implicated in the regulation of neurotransmitter release and excitability of neuronal networks. Mutation of synapsin genes in mouse and human causes epilepsy. To understand the role of the highly conserved synapsin domain E in the dynamics of release from mammalian inhibitory neurons, we generated mice that selectively overexpress the most conserved part of this domain in cerebellar Purkinje cells. At Purkinje-cell–nuclear-neuron synapses, transgenic mice were more resistant to depression induced by short or prolonged high-frequency stimulations. The increased synaptic performance was accompanied by accelerated release kinetics and shorter synaptic delay. Despite a marked decrease in the total number of synaptic vesicles, vesicles at the active zone were preserved or slightly increased. The data indicate that synapsin domain E increases synaptic efficiency by accelerating both the kinetics of exocytosis and the rate of synaptic vesicle cycling and decreasing depression at the inhibitory Purkinje-cell–nuclear-neuron synapse. These effects may increase the sensitivity of postsynaptic neurons to inhibition and thereby contribute to the inhibitory control of network activity.

Key words: Synaptic vesicle release, Exocytosis, Synapsin, Synaptic plasticity, Cerebellum, Transgenic

Introduction

Information transfer between neurons is controlled by an efficient process of regulated exocytosis of neurotransmitters stored in synaptic vesicles (SVs). In nerve terminals, SVs are organized in distinct functional pools, a large reserve pool (RP) in which SVs are restrained by the actin-based cytoskeleton, an actively recycling pool and a quantitatively smaller readily releasable pool (RRP) in which SVs are free to approach the presynaptic active zone and fuse with it upon stimulation (Rizzoli and Betz, 2005). Synapsins, a family of abundant SV-associated phosphoproteins (Greengard et al., 1993; Hilfiker et al., 1999), play a prominent role in the regulation of SV trafficking and their involvement in human pathology, namely epilepsy, has been recently recognized (Garcia et al., 2004). Synapsins regulate the pre-docking steps of exocytosis by anchoring SVs to the actin cytoskeleton and regulating their availability for exocytosis through their phosphorylation-induced dissociation from SVs and/or actin filaments (Benfenati et al., 1992a; Benfenati et al., 1992b; Ceccaldi et al., 1995; Jovanovic et al., 1996; Hosaka et al., 1999; Chi et al., 2001; Chi et al., 2003; Bonanomi et al., 2005). Moreover, synapsins have been reported to play additional roles in the later steps of neurotransmitter release, including priming and fusion (Hilfiker et al., 1998; Hilfiker et al., 2005; Humeau et al., 2001).

Synapsins are encoded by three genes (*SYN1*, *SYN2* and *SYN3*) in mammals (Südhof et al., 1989; Porton et al., 1999) and alternative splicing of these genes gives rise to at least eight different isoforms composed of a mosaic of individual and common domains, the latter of which (domains A, C and E) are highly conserved evolutionarily from invertebrates to man (Kao et al., 1999). In particular, the C-terminal domain E, shared by all A-type synapsin isoforms, plays a fundamental role in synapsin function. Indeed, it is implicated in both the pre-docking and the post-docking steps of synaptic vesicle exocytosis (Pieribone et al., 1995; Hilfiker et al., 1998; Hilfiker et al., 2005) and appears to be required for the correct targeting of the synapsins to synaptic vesicles (Gitler et al., 2004a). However, thus far the exact role of domain E in neuroexocytosis has never been investigated in mammalian synapses. In synapsin knockout mice epilepsy seems to be caused by a specific deficit in inhibitory transmission (Li et al., 1995; Rosahl et al., 1995; Terada et al., 1998; Gitler et al., 2004b) and domain E is deleted in the truncation mutant of synapsin I found in X-linked human epilepsy (Garcia et al., 2004), it therefore seemed important to investigate the precise role of the synapsin domain E in mammalian inhibitory synapses.

To this aim, we generated cell-specific transgenic mice that

selectively overexpress the most conserved part of the E domain (pepE) in cerebellar Purkinje cells (PCs). The results indicate that, notwithstanding a decrease in the RP of SVs, the endogenous expression of this peptide increases the performance of the inhibitory PC deep cerebellar nuclei (DCN) synapse by accelerating the kinetics of neurotransmitter release and making the synapse less susceptible to depression.

Results

Generation of L7-pepE mice

The C-terminal part of the synapsin domain E is remarkably conserved among mammalian A-type isoforms and in synapsin orthologues throughout the animal kingdom. To address the question of the functional role of this sequence in mammalian synapses, we specifically overexpressed it in a single neuronal population. A minigene was made by hybridization of two complementary oligonucleotides and cloned into the PC-specific expression vector L7ΔAUG. When expressed, the minigene was expected to induce a 25-mer peptide, corresponding to the last 25 residues of domain E from rat and mouse synapsins Ia (Fig. 1A). After injection of the L7-pepE construct into zygotes derived from the hybrid mouse strain C57Bl6×DBA2, four positive transgenic mouse lines (Tg-1 to Tg-4) were identified by PCR analysis (Fig. 1B). Two lines (Tg-1 and Tg-2) were amplified, crossed to homozygosity and bred through at least eight generations. Reverse transcriptase (RT)-PCR analysis on total RNA extracted from cerebellum, cerebral cortex and corpus striatum demonstrated that the L7-pepE transgene was expressed only in the cerebellum of both lines of L7-pepE transgenic mice (Fig. 1C and data not shown). Consistently, in situ hybridization experiments revealed that the transgene mRNA was specifically, abundantly and homogeneously expressed in the PC layer of the cerebellar cortex (Fig. 1D). No detectable expression was observed in any other brain region, except for the retina (not shown), and an identical pattern of expression was observed in both Tg-1 and Tg-2 mice.

Cerebellar structure and PC terminals at DCN are normal in L7-pepE mice

The gross morphology of the brains from transgenic mice was virtually identical to that of their control littermates. Basic histological analysis with Nissl staining showed that the cerebellum of transgenic mice was normal in size and external appearance with regular foliation and layering of the cerebellar cortex (Fig. 2A, panels a,b). As in control animals, PCs of L7-pepE mice specifically labelled for calbindin D-28K had a characteristic morphology and displayed a typical dendritic tree in the molecular layer, the expected cell-body density in the PC layer and regular projections to the DCN (Fig. 2A, panels c-f). Thus, pepE overexpression in PCs had no detectable effect of cerebellar structure and PC differentiation and maturation.

When cerebellar sections were double stained with calbindin D-28K and anti-peptide E or anti-synapsin I antibodies, synapsin immunoreactivity exhibited a comparable

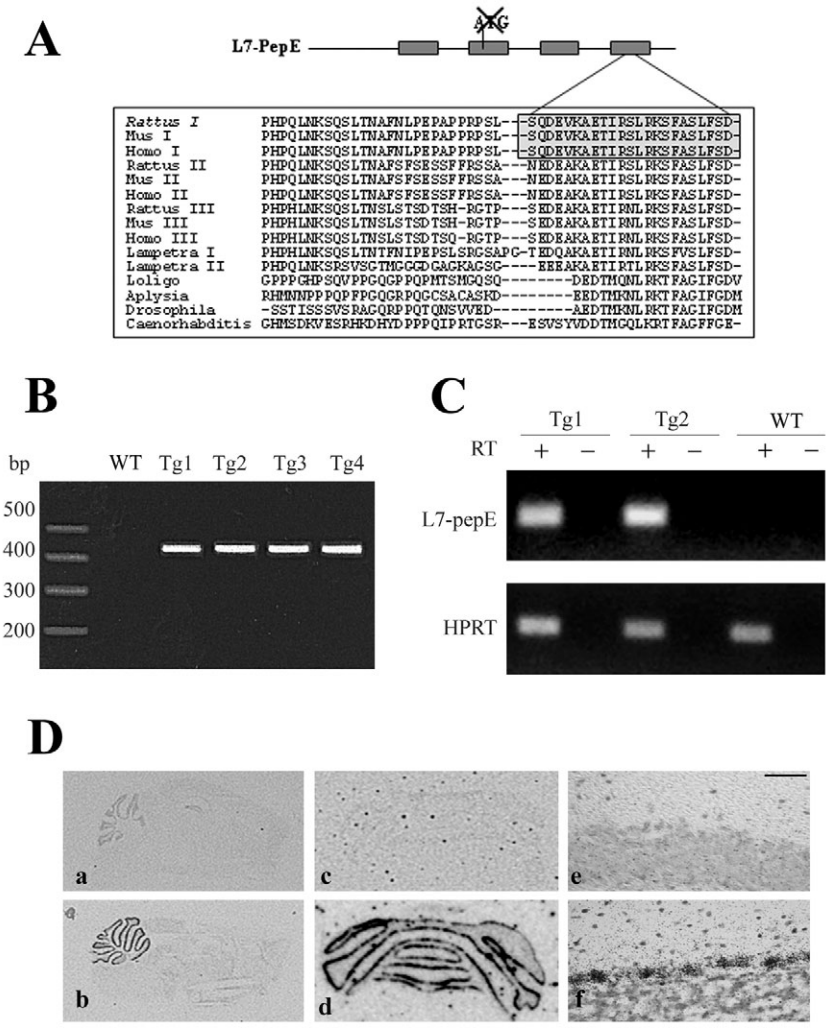

Fig. 1. Construction and PC-specific expression of the L7-pepE transgene. (A) The L7-pepE transgene was made by insertion of a synthetic mini-gene coding for the highly conserved 25 C-terminal amino acids of synapsin Ia (pepE; see box) into the L7ΔAUG vector. (B) PCR analysis of DNA prepared from tail biopsies revealed insertion of the transgene in four distinct transgenic (Tg-1, Tg-2, Tg-3, Tg-4) mouse lines. WT, wild-type. (C) The expression of the L7-pepE transgene was assessed by RT-PCR experiments performed on total RNA prepared from the cerebella of wild-type (wt) and two L7-pepE (Tg-1 and Tg-2) mouse lines. Samples that were not incubated with reverse transcriptase (RT) are shown as negative controls. HPRT was used as an internal control. (D) In situ hybridization was performed on sagittal (a,b) or coronal (c-f) sections from the brains of wild-type (a,c,e) and Tg-1 (b) or Tg-2 (d,f) transgenic mice using a ^{35}S-labelled L7-pepE antisense oligonucleotide probe. The hybridization signal, undetectable in wild-type sections, is intense in transgenic sections and exclusively restricted to the cerebellar cortex. At higher magnification (e,f), grains counterstained with cresyl violet are concentrated in PC somata. Bars, 2.8 mm (a,b); 1.2 mm (c,d); 100 μm (e,f).

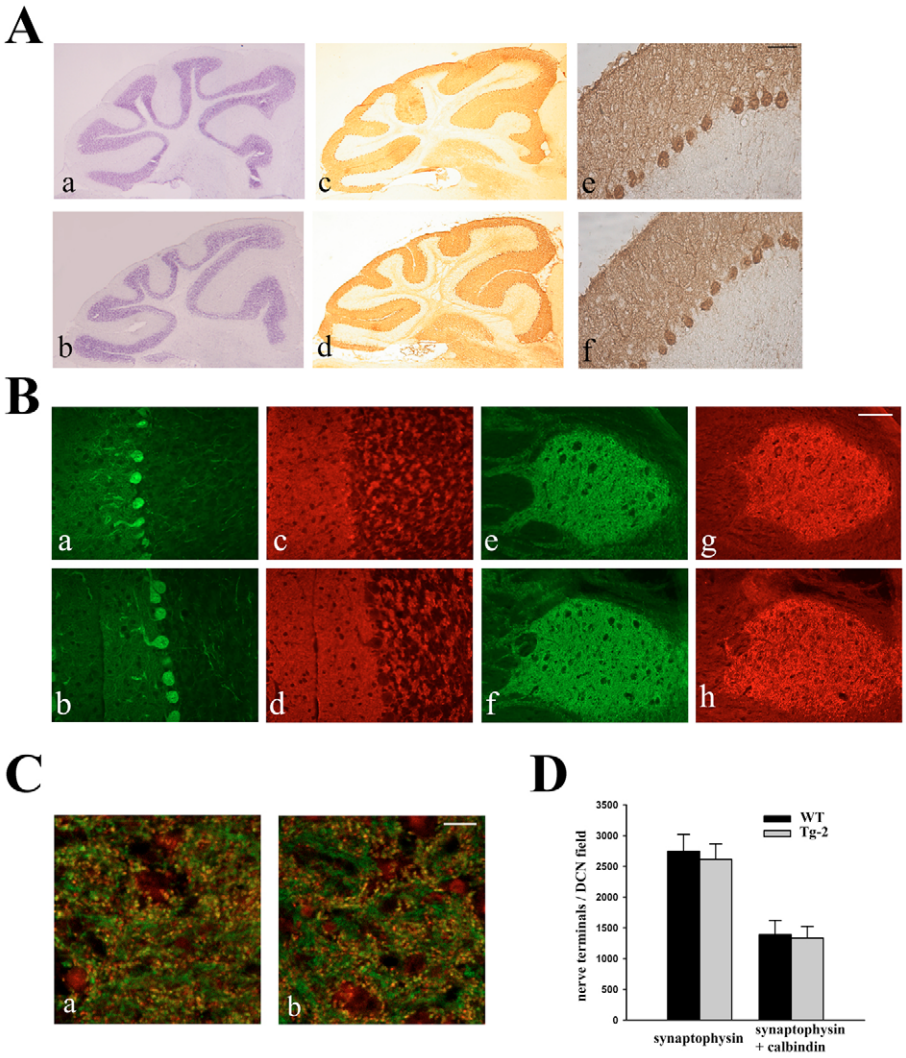

Fig. 2. Cerebellar anatomy and innervation of DCN neurons by Purkinje cells are preserved in L7-pepE mice. (A) Sections of wild-type (a,c,e) and Tg-2 (b,d,f) mice were stained with Cresyl Violet (a,b) or with an anti-calbindin D-28K antibody (c-f). The cerebella of transgenic and control mice are indistinguishable when considering size, foliation, layering of cerebellar cortex, morphology, density and arrangement of PC. Bar, 600 μm (a-d); 100 μm (e,f). (B) Double immunofluorescence with anti-calbindin D-28K (a,b,e,f) and anti-synapsin pepE (G304; c,d,g,h) antibodies in cerebellar sections from wild-type (a,c,e,g) and Tg-2 (b,d,f,h) mice. Synapsin pepE immunoreactivity in the cerebellar cortex (a-d) and DCN (e-h) of both groups has a typical distribution with intense staining of the molecular layer, negative PC somata and intense staining at the granule cell layer and in the DCN. Bar, 100 μm (a-d); 200 μm (e-h). (C) High magnification of wild-type (a) and Tg-2 (b) sections double-immunostained with anti-calbindin D-28K (green) and anti-synaptophysin (red) antibodies. PC terminals appear yellow because of the positive staining for both antibodies. Bar, 10 μm. (D) Number (mean ± s.e.m.) of synaptophysin-positive terminals and calbindin- and synaptophysin-positive terminals (PC terminals) in the DCN was calculated as described in Materials and Methods (n=4 per genoptype). PC nerve terminals represented 49±3.7% (means ± s.e.m.; n=4) and 51±2.7 (means ± s.e.m.; n=4) of total synaptophysin-positive DCN terminals in wild-type and Tg-2 mice, respectively.

distribution pattern in both transgenic and control mice, with intense labelling of the molecular and granule cell layer, 'negative' appearance of the PC somata (Fig. 2B, panels a-d) and intense punctate staining in the DCN (Fig. 2Be-h; Fig. 2C). Moreover, the number of synaptophysin- and calbindin-positive PC terminals impinging on DCN neurons was virtually unchanged in L7-pepE mice (Fig. 2C,D). Although it was not possible to distinguish between pepE and endogenous synapsin, no pepE immunoreactivity was detected in PC somata, suggesting that the recombinant peptide was transported to nerve terminals together with endogenous synapsins (Gitler et al., 2004a).

To demonstrate unambiguously that pepE is expressed and correctly targeted to axonal and nerve terminal domains in transgenic PC, we enriched PCs from the cerebellum of embryonic day (E)18 Tg-2 mice and analyzed the expression of synapsin I and pepE by immunocytochemistry and immunoblotting. Immunoblotting confirmed that both synapsin I and pepE are expressed in PC-enriched cerebellar cultures; in addition, the absence of both proteins in PC cell bodies indicates that pepE is transported to nerve terminals (Fig. 3A,B). The demonstration that this is indeed the case was obtained by transfecting primary hippocampal neurons with either GFP or the GFP chimeras of synapsin Ia or domain E (Fig. 3C,D). Synapsin Ia or domain E GFP chimeras revealed a punctate distribution pattern largely overlapping with the immunoreactivity for the synaptic vesicle protein VAMP2, whereas the distribution of GFP alone was fully cytosolic.

L7-pepE mice have an impaired motor performance

Mice in both lines were viable, fertile and showed weight, growth, life expectancy and general motor activity comparable with wild-type littermates. Visual inspection of Tg-1 and Tg-2 mice did not reveal any gross alteration in behaviour with respect to wild-type mice. Footprints of L7-pepE mice showed no evidence of an ataxic phenotype. Step width, step length and maximum difference in stride length in transgenic mice were not statistically different from those of control littermates (Fig. 4A).

In the horizontal bar test, which evaluates dynamic balance, both wild-type and transgenic mice performed well, whereas in the vertical bar test, which evaluates static balance, both Tg-1 and Tg-2 mice obtained a significantly lower score than wild-type mice (Fig. 4B). Although transgenic animals did not fall during the 60 seconds of the test, they stayed gripped to the

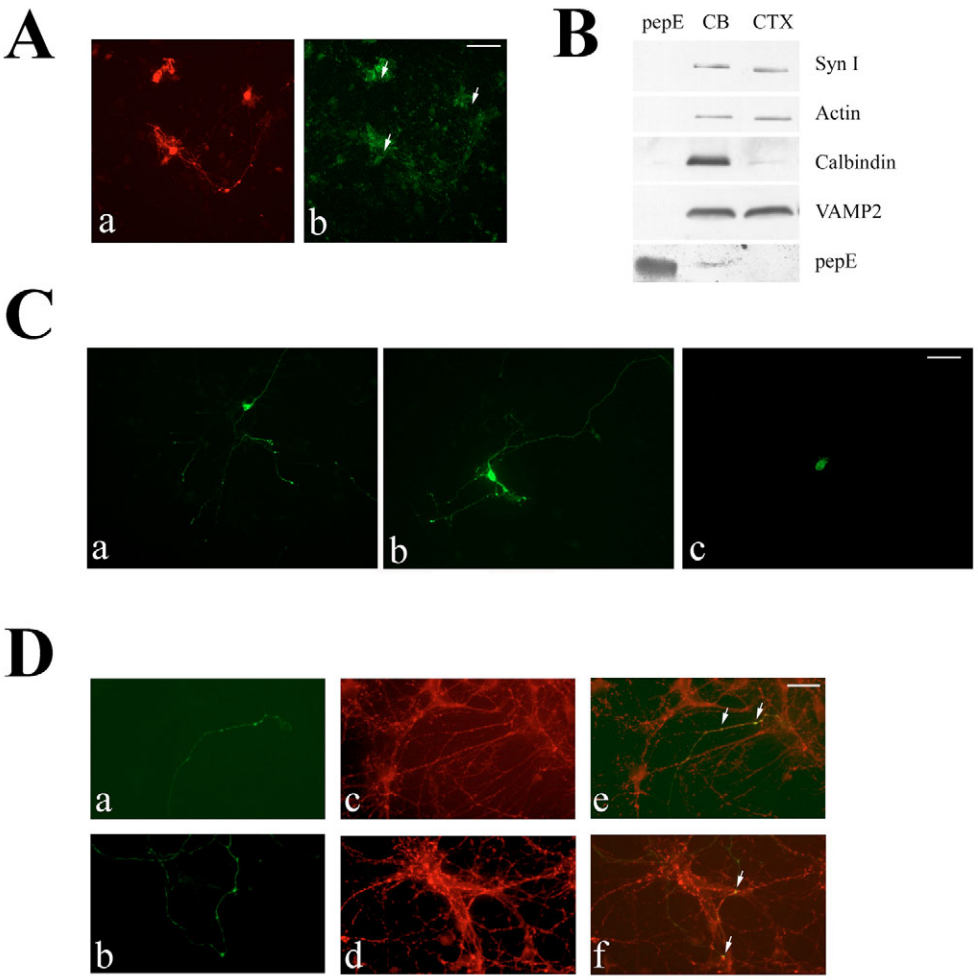

Fig. 3. The recombinant pepE is expressed in Purkinje cells and is targeted to nerve terminals. (A) Tg-2 PC double immunostained for calbindin (a) and pepE (b). PepE immunoreactivity is absent from the cell body (arrow) and concentrated in presynaptic boutons. Bar, 100 μm. (B) Primary cerebellar (CB) and neocortical (CTX) cultures from Tg-2 mice were solubilized at 8-10 DIV and subjected to Tris-tricine SDS-PAGE. Expression of synapsin I (10.22 antibody; Syn I), actin, calbindin, VAMP2 and recombinant pepE (G304 antibody) is shown. The first lane on the left contained synthetic pepE (50 ng). (C) Primary wild-type hippocampal neurons were transfected to overexpress either GFP-synapsin Ia (a), GFP-domain E (b) or GFP alone (c). Bar, 200 μm. (D) Expression and targeting of GFP-synapsin Ia (a) or GFP-domain E (b) were followed by counterstaining neurons with VAMP2 antibodies (c,d). Both synapsin Ia and domain E GFP chimeras are transported along the axon and localized in en-passant varicosities and VAMP2-positive axon terminals (see arrows in e,f). Bar, 100 μm.

pole, whereas wild-type animals climbed up and down and finally got off the pole.

The ability to maintain balance on a rotating cylinder and to adapt to the rate of locomotor activity was assayed by using the rotarod test. In the constant speed mode, wild-type and transgenic mice performed equally well when the rotation speed was slow or moderately high (up to 30 rpm). However, at the maximum speed (40 rpm) both Tg-1 and Tg-2 mice displayed a statistically significant impairment in motor performance (Fig. 4C). Although wild-type mice exhibited an increased performance along successive training sessions in the accelerating mode, Tg-2 mice displayed no significant improvement in motor performance (Fig. 4C, inset). These results indicate that pepE overexpression resulted in a mild, but significant, motor impairment in balance, coordination and motor learning that becomes apparent under the most demanding conditions.

[^{3}H]GABA release in response Ca^{2+} ionophores, but not depolarization, is impaired in L7-pepE PC terminals

To determine whether the impairment in motor performance observed in L7-pepE mice was generated by a modification at the level of PC-DCN synapse, we analyzed neurotransmitter release from PC.

Release experiments were conducted on DCN synaptosomes labelled with [^{3}H]GABA and stimulated with KCl, known to evoke voltage-gated Ca^{2+}-channel-dependent release, mainly involving the RRP of SVs, or with ionomycin, known to diffusely increase intrasynaptosomal Ca^{2+} concentration and induce massive SV exocytosis, involving the RP of SVs (Ashton and Dolly, 2000; Stigliani et al., 2003). As shown in Fig. 5A, KCl-induced [^{3}H]GABA overflow was similar in synaptosomes from wild-type, Tg-1 or Tg-2 mice. By contrast, ionomycin-induced [^{3}H]-GABA overflow was significantly reduced by about 30-40% in both lines of transgenic mice with respect to control mice (Fig. 5B). These results indicate that overexpression of pepE reduces the availability of reserve SVs in PC nerve terminals, whereas the RRP of SVs seems not to be impaired.

Since PC neurons are known to experience sustained high-frequency firing, a condition that could involve slow SV cycling between the RP and the RRP, synaptosomes were stimulated with three sequential depolarizing pulses with 15 or 35 mM KCl. As expected, in wild-type synaptosomes, [^{3}H]GABA overflows decreased in response to the progressive stimuli, as a result of SV depletion and decreased [^{3}H]-GABA specific activity of neurotransmitter quanta. Surprisingly, GABA overflow in Tg-1 and Tg-2 synaptosomes was significantly less depressed after repetitive pulses (Fig. 5C), indicating that pepE-overexpressing PC terminals have a more efficient refilling of the RRP following intense repetitive stimuli.

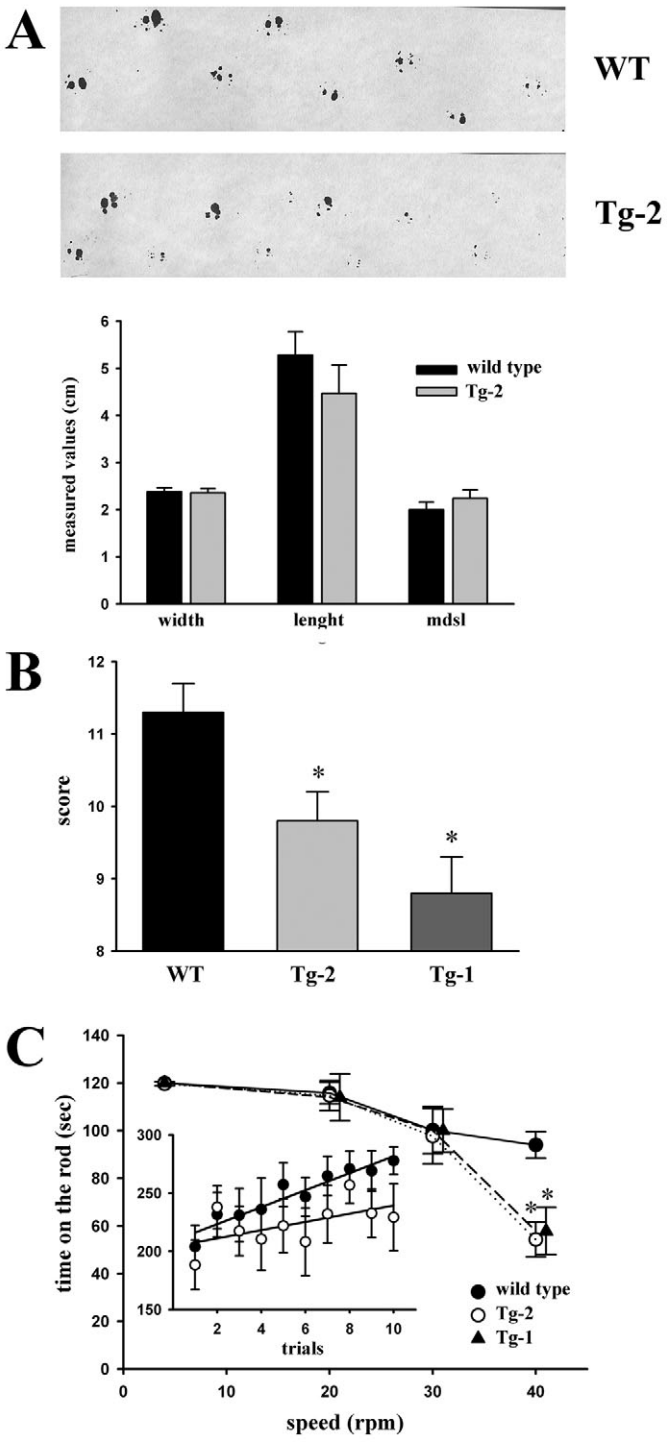

Fig. 4. Motor coordination is altered in L7-pepE mice. (A) Upper panel, representative footprint patterns of a wild-type and a L7-pepE mouse. Lower panel, comparison of step widths, step lengths and maximum differences in stride length (mdsl) between wild-type (black bars; *n*=20) and Tg-2 (grey bars; *n*=20) animals. Locomotion is similar in both groups and no ataxic phenotype is observed. (B) Vertical pole scores (means ± s.e.m.), recorded as described in Materials and Methods, are reported for wild-type (black bars; *n*=23), Tg-2 (light grey bars; *n*=23) and Tg-1 (dark grey bars; *n*=10) mice. Each animal was tested in three consecutive trials. **P*<0.05, Newman-Kleus multiple comparison test. (C) Rotarod performance of wild-type (●, *n*=9), Tg-1 (▲, *n*=9) and Tg-2 (○, *n*=8) mice in the constant speed mode. The time (means ± s.e.m.) mice remained on the rotating rod at the various speeds are reported. **P*<0.05, Newman-Kleus multiple comparison test. Inset, rota-rod motor learning of wild-type (●, *n*=10) and Tg-2 (○, *n*=10) mice in the constant acceleration mode. Individual learning curves were fitted using linear regression [Y-intercept, 162±19 for WT mice and 151±19 for Tg-2 mice (*P*=0.7); slope, 11.2±3.3 for wild-type mice and 1.5±2.9 for Tg-2 mice (*P*<0.05)]. The performances in the initial and final trials of the learning curve were significantly different only in wild-type mice (*P*<0.005), but not in Tg-2 mice (*P*=0.26, Student's *t* test).

Synaptic depression is decreased in PC-DCN synapses from L7-pepE mice

To investigate synaptic transmission at the PC-DCN synapse, we performed electrophysiological experiments in acute cerebellar slices using whole-cell patch-clamp recordings from postnatal day (P)8-P12 wild-type and Tg-2 mice. DCN neurons showed a continuous barrage of spontaneous inhibitory postsynaptic currents (IPSCs) (wild-type mice, 33.6±12.9 IPSCs/second; *n*=9) (Tg-2 mice, 50.8±12.8 IPSCs/second; *n*=7; *P*=0.25 compared with level in wild type) reflecting tonic discharge in PCs (Anchisi et al., 2001). Since evoked IPSCs (wild type, 754.9±303.5 pA; *n*=9) (Tg-2, 679±241.7 pA; *n*=7; *P*=0.85) were larger than spontaneous IPSCs (wild type, 94.0±25.8 pA; *n*=9) (Tg-2, 51.8±9.0 pA; *n*=7; *P*=0.2), they were multi-fiber in nature (Telgkamp and Raman, 2002).

In a first set of experiments, PC axons were stimulated with a train of 20 impulses at 100 Hz to assess processes involving fast SV cycling (Fig. 6A). In control slices, IPSC amplitude declined with an exponential time course (Fig. 6B), revealing short-term synaptic depression very similar to that reported previously (Telgkamp and Raman, 2002; Pedroarena and Schwarz, 2003; Telgkamp et al., 2004). The same stimulation paradigm applied on Tg-2 slices elicited smaller depression (Fig. 6A), with a slower rate and a higher steady-state level with respect to wild-type slices (Fig. 6B). As shown in Fig. 6C, the time constant and the steady-state level of depression increased threefold and twofold, respectively, in Tg-2 versus wild-type synapses. The depression time constant changed from 13.9±2.3 milliseconds (*n*=4) in the wild type to 45.7±8.2 milliseconds (*n*=4) in Tg-2 mice (*P*<0.05, unpaired *t*-test). The steady-state level changed from 12.3±5.0% (*n*=4) in the wild type to 22.9±1.5% (*n*=4) in Tg-2 mice (*P*<0.05, unpaired *t*-test). The presynaptic nature of depression was supported by the appearance of failures in the last IPSC in the trains (wild type, 56.6±10.4%; *n*=4) (Tg-2, 23.1±12.9; *n*=3; see also below), as previously reported (Telgkamp and Raman, 2002; Pedroarena and Schwarz, 2003; Telgkamp et al., 2004).

In a second set of experiments, PC axons were stimulated at 50 Hz for 120 seconds. During such prolonged trains, which should involve slower and longer pathways of SV recycling, depression was also slower and less intense in Tg-2 compared with wild-type synapses (Fig. 7A,B). The steady state of mean IPSC amplitude was 1.95±0.4% (*n*=5) in wild-type synapses and 3.96±1.8% (*n*=5) in Tg-2 synapses ($P<10^{-11}$, ANOVA). Depression was associated with a marked increase in IPSC failures, which caused a lower steady state than in short trains (cf. Fig. 5B) supporting the presynaptic nature of the difference (Fig. 7B). The steady state of failure frequency was 83.4±3.8%

(n=5) in wild-type and 69.0±3.9% (n=5) in Tg-2 synapses ($P<10^{-7}$ using χ^2 test).

It should be noted that in these experiments DCN neurons were maintained at negative membrane potential. Under these conditions, the previously reported forms of long-term synaptic plasticity of the PC-DCN synapse (Morishita and Sastry, 1996; Ouardouz and Sastry, 2000; Aizenmann et al., 1998) were very unlikely to occur because they require membrane depolarization. Moreover, to rule out the possibility that pepE overexpression affects PC spike firing, PC recordings performed at P15 revealed comparable spontaneous PC discharge frequencies in wild-type (5.05±0.67 Hz; n=12) and Tg-2 L7-pepE (5.22±0.40 Hz; n=14) slices (P=0.83, unpaired Student's t-test).

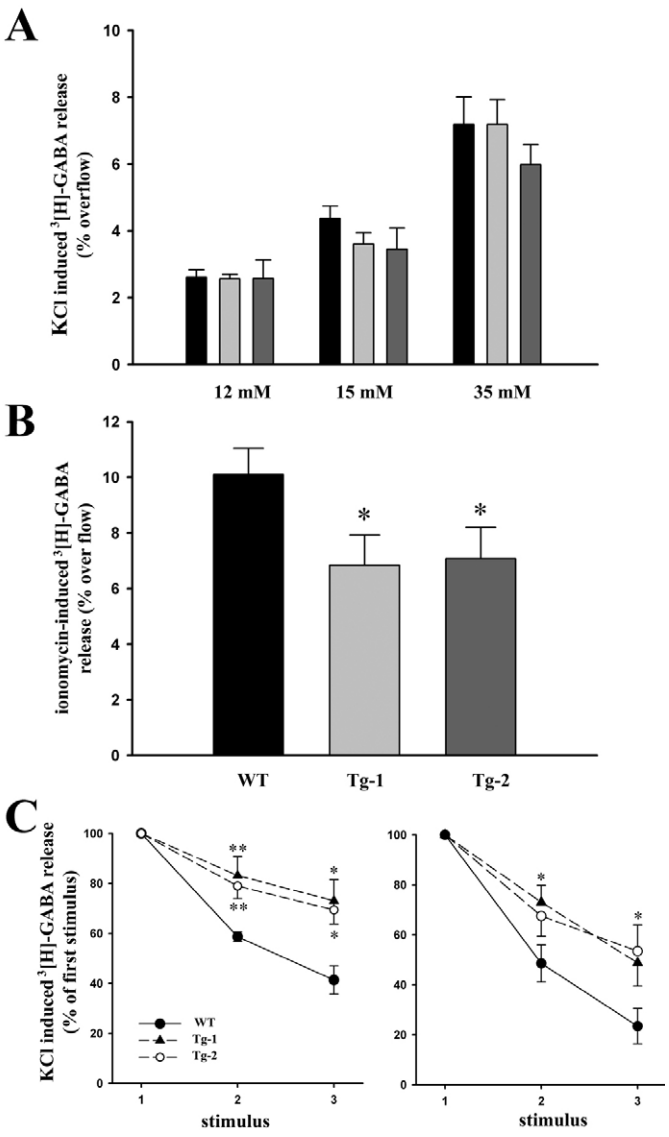

Fig. 5. [^{3}H]-GABA release from L7-pepE DCN synaptosomes is impaired in response to ionomycin, but it is more efficient after repetitive depolarization. (A) DCN synaptosomes from wild-type (black bars), Tg-1 (light grey bars) and Tg-2 (dark grey bars) were depolarized with 12, 15 or 35 mM KCl. Results are expressed as stimulus-evoked overflow, means ± s.e.m. of 5-10 independent experiments. (B) DCN synaptosomes from wild-type, Tg-1 and Tg-2 mice were treated as in A, except that [^{3}H]-GABA release was induced by 0.5 μM ionomycin. Bars are means ± s.e.m. of 6-8 independent experiments. *P<0.05, Dunnett's multiple comparison test vs wild-type. (C) DCN synaptosomes from wild-type (●), Tg-1 (▲) and Tg-2 (○) mice were treated as in A and subjected to three sequential depolarizing pulses with either 15 mM (left panel) or 35 mM (right panel) KCl. [^{3}H]-GABA release evoked by each pulse is expressed in percent of the release evoked by the first stimulus (means ± s.e.m. of four to five independent experiments). *P<0.05 and **P<0.001, one way ANOVA followed by Duncan's multiple comparison test.

The kinetics of GABA release from L7-pepE PC terminals is accelerated

A further indication for a role of pepE in the regulation of RRP dynamics came from measurements of the time course of single IPSCs and of the synaptic delay in PC-DCN synapses of wild-type and Tg-2 mice. As shown in Fig. 8A,C, the IPSC rise and decay times were significantly reduced in transgenic nerve terminals (wild type rise time, 1.5±0.2 milliseconds; n=9; decay time, 17.4±3.0 milliseconds; n=7) (Tg-2 rise time, 1.0±0.1 milliseconds; n=7; P<0.05; decay time, 9.6±0.9 milliseconds; n=7; P<0.05). Moreover, the synaptic delay was significantly shorter in Tg-2 (1.4±0.1 milliseconds; n=7) compared with wild-type synapses (1.9±0.2 milliseconds; n=9; P<0.05). The large and consistent differences in synaptic delay (about 500 μseconds) observed between wild-type and Tg-2 mice are unlikely to be attributable to changes in the distance between stimulating and recording electrodes, since the stimulating electrode was always placed within 100±20 μm from recorded DCN cells and, with an estimated conduction velocity of PC axons of 0.7 m/second (Clark et al., 2005), the jitter of delay would be only ±28 μseconds. Although the possibility of different conduction velocity or axon tortuosity cannot be excluded, no changes in synaptic morphology supporting a longer or slower diffusion of GABA were detected in transgenic mice (see Fig. 2C and Table 1). These data imply that the time needed to release a SV is

Table 1. Morphometric analysis of PC terminal ultrastructure

Parameter	Wild type (n=3)	Transgenic (n=3)
Synapse area (μm^2)	1.14±0.10	1.13±0.09^{NS}
AZ length (μm)	0.43±0.03	0.44±0.02^{NS}
SV/synapse	153±10	88±6**
SV<200 nm from AZ or synapse	19.1±1.3	22.8±3.2^{NS}
SV>200 nm from AZ or synapse	134±10	65±3***
Mean distance from AZ	658±48	431±18**
SV<200 nm from AZ	122±3	116±4^{NS}
SV>200 nm from AZ	732±47	549±13*
Mean intervesicular distance	771±51	650±26^{NS}
Mean clustering index	0.88±0.05	1.05±0.01*

Parameters (means ± s.e.m.) were calculated from the EM images of 60 and 54 synapses from three wild-type and three Tg-2 mice, respectively. Individual PC-DCN synapses were analyzed as described in Materials and Methods to give mean individual values. Statistical analysis was performed using the unpaired Student's t-test. *P<0.05; **P<0.01; ***P<0.0005; NS, not significant. AZ, active zone; SV, synaptic vesicles. The clustering index was calculated, for each synapse, as the ratio between the predicted intervesicular distance for a homogeneously distributed vesicle population and the measured intervesicular distance.

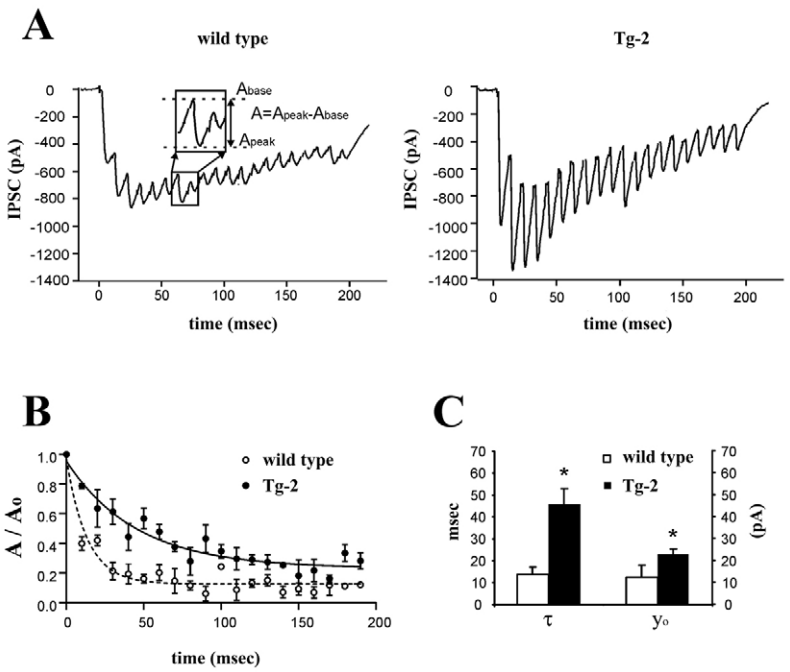

Fig. 6. Depression induced by short trains at 100 Hz is less intense in L7-pepE mice. (A) Whole-cell patch-clamp recordings of P8-P10 DCN neurons from wild-type (left panel) and Tg-2 (right panel) mice. IPSC trains were obtained by stimulating PC axons at 100 Hz for 200 milliseconds. Facilitation is apparent and depends on temporal summation of IPSCs. Each train is the average of ten tracings to reduce synaptic variability. (B) Average of independent recordings performed as described above in wild-type (○, n=4) and Tg-2 (●, n=4) mice. Amplitudes were normalized to the first IPSC and fittings were performed with an exponential function of the form $y(t)=A\times e^{-t/\tau}+y_0$. Note the slower depression and the higher steady-state level observed in mutant animals. (C) Time constant (τ) and steady-state amplitude (y_0) of depression are shown as means ± s.e.m. for wild-type (white bars; n=4) and Tg-2 (black bars; n=4) mice. *P<0.05, Student's unpaired t test.

reduced, consistent with an involvement of pepE in the reactions that determine kinetics and synchronization of quantal release.

PC nerve terminals exhibit changes in the number and distribution of SVs

To ascertain whether the changes in synaptic physiology observed in PC-DCN synapses were associated with differences in synaptic structure and/or SV distribution, PC terminals making axo-somatic synapses on nuclear neurons were analyzed by electron microscopy. PC terminals from transgenic mice showed a marked decrease in the total number of SVs compared with wild-type terminals (Fig. 9A and Table 1). In the absence of detectable differences in both the average synaptic area and active zone number and length, the total number of SVs per synapse in Tg-2 mice was ~55% of that of wild-type mice.

The extent of clustering of SVs in PC nerve terminals from transgenic and control mice was deduced from the mean intervesicular distance (MID) corrected for the SV density (clustering index, see Materials and Methods). Despite a decrease in the number of SVs, the overall MID was lower in

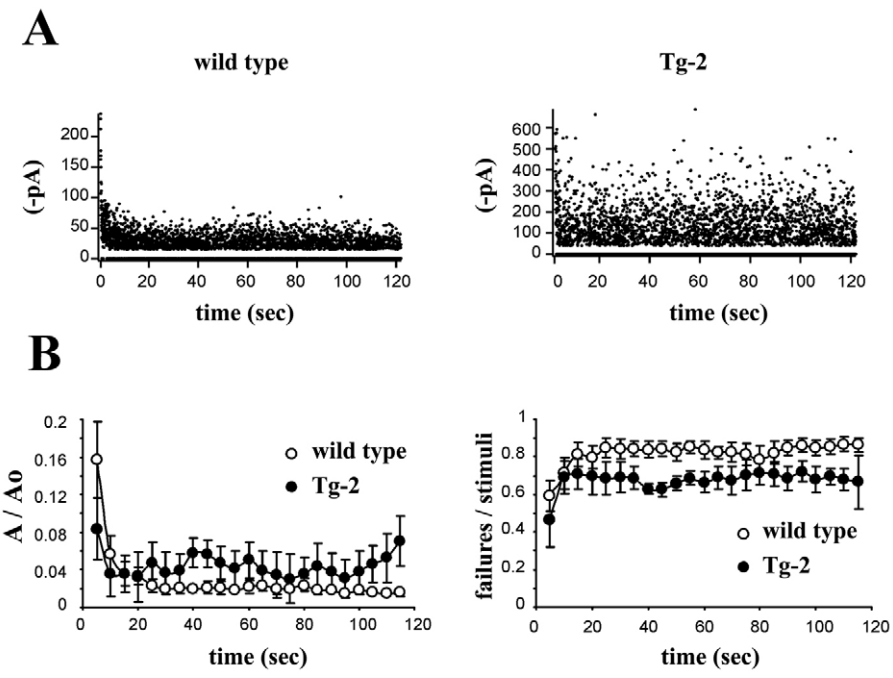

Fig. 7. L7-pepE PC terminals exhibit milder depression and faster recovery after prolonged high-frequency stimulation. (A) Effect of prolonged stimulation trains (50 Hz for 2 minutes) on IPSC amplitude. A representative experiment shows the faster and more intense synaptic depression in wild-type mice (left) with respect to Tg-2 mice (right). (B) Left panel, IPSC amplitudes during the prolonged stimulation are expressed in percent of the first IPSC. The IPSC decrease was smaller in L7-pepE (●, n=4) than in wild-type (○, n=5) mice. Statistical analysis was performed on the steady-state levels (50-120 seconds) using the Student's unpaired t test ($P<10^{-8}$). Right panel, the number of failures during prolonged stimulation trains was lower in L7-pepE (●, n=4) than in wild-type (○, n=5) mice. Data are reported as means ± s.e.m. Statistical analysis was performed on the steady-state levels (50-120 seconds) using the Student's unpaired t test ($P<10^{-13}$).

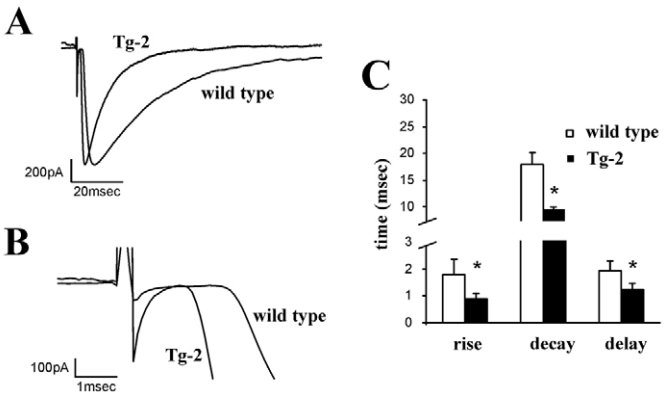

Fig. 8. The kinetics of release is faster in L7-pepE mice. (A) Representative IPSCs recorded from DCN neurons from wild-type and Tg-2 mice. IPSC traces were normalized to identical peak amplitudes. (B) Representative IPSCs recorded from PC-DCN synapses showing the shortening of the synaptic delay in IPSC in Tg-2 mice with respect to wild-type mice. (C) The histogram shows the mean values (± s.e.m.) for IPSC rise, decay and delay times obtained from wild-type (white bars; n=9) and Tg-2 (black bars; n=7) mice. IPSC rise time was measured as the time needed to rise from 10% to 90% of peak amplitude. IPSC decay time was evaluated by exponential fitting of the decay with the exponential function $y(t)=A\times e^{-t/\tau}$. Statistical analysis was performed using the Student's unpaired t test; *P<0.05.

transgenic mice, resulting in a significantly higher clustering index with respect to wild-type mice (Table 1). In addition, SVs were more concentrated in proximal shells, as shown by a significant decrease in the mean distance from the active zone (Table 1 and inset of Fig. 9B).

A detailed morphometric analysis of SV distribution within PC terminals (Fig. 9B) indicated that the decrease in SV density was highly significant at distances between 400 and 1400 nm from the active zone. These data are consistent with previous results obtained after injection of pepE in invertebrate excitatory synapses and can explain the decreased response in GABA release to ionomycin observed in transgenic animals. Interestingly, SVs within 200 nm of the active zone were totally preserved or even slightly increased, reaching significance (P<0.05) in the 50-100 nm shell.

Discussion

To investigate the functional role of the highly conserved domain E of synapsin in a central inhibitory synapse, we selectively overexpressed the most conserved sequence of the domain in cerebellar PC in two independent transgenic lines. The recombinant peptide was expressed at detectable levels, was virtually absent from PC somata and was correctly targeted to nerve terminals in the presence of endogenous synapsins, consistent with a positive role of this domain in synapsin targeting to nerve terminals (Gitler et al., 2004a). Despite an

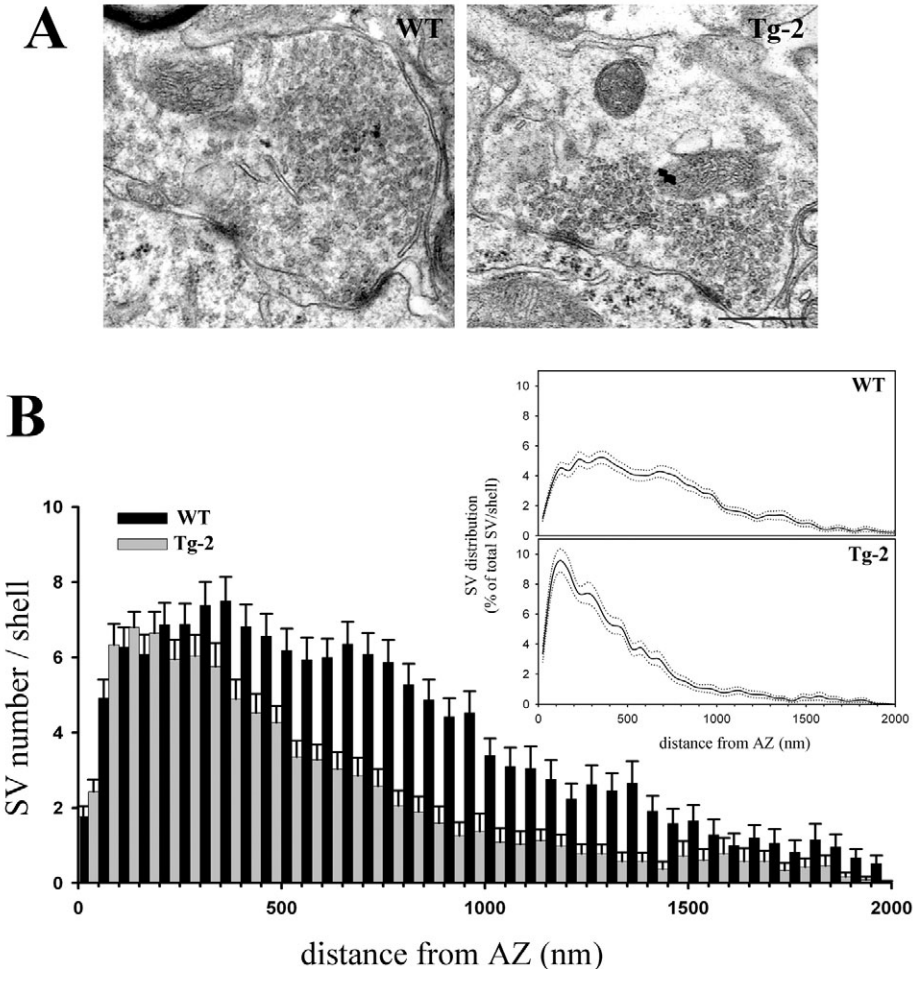

Fig. 9. SV density and distribution is altered in L7-pepE mice. (A) Representative electron micrographs of PC terminals on DCN somata from wild-type (WT, left panel) and Tg-2 (right panel) mice. Bar, 1 μm. (B) Distribution of SVs in PC terminals from wild-type (black bars; n=60) and Tg-2 (grey bars; n=54) mice. The absolute number of SVs (means ± s.e.m.) located within successive 50 nm shells from the active zone (AZ) is shown. The frequency distribution of SVs as a function of the distance from the AZ was analyzed using the Kolgomorov-Smirnov and Mann-Whitney tests; P<0.05 for the 50-100 nm shell; P<0.01 for the intervals between 400 and 1400 nm. Inset, to analyze the distribution pattern of SVs, the number of SVs in the various shells was expressed in percent of the total SV number for each PC terminal of wild-type (WT, upper panel) and Tg-2 (lower panel) mice. The solid traces and dotted lines represent the mean and s.e.m. values, respectively.

impaired motor performance, transgenic mice had a normal cerebellar structure, PC morphology and density of PC terminals onto DCN neurons. Interestingly, PC terminals of L7-pepE mice displayed an accelerated kinetics of exocytosis and a marked resistance to depression evoked by high-frequency stimulation. This increased synaptic performance was associated with a marked decrease in the number of SVs away from the active zone, whereas SVs close to the active zone were preserved or slightly increased.

The phenotype of L7-pepE mice points to a specific role of the synapsin domain E in the regulation of SV trafficking at both pre- and post-docking steps, involving both the RP and the RRP of SVs. In both the squid giant synapse (Hilfiker et al., 1998) and mammalian PC-DCN synapses (this study), overexpression of pepE induced a marked depletion of SVs in the RP, leaving the RRP virtually unaffected. This effect is in agreement with the inhibition of the actin and synapsin interactions by pepE recently reported by our laboratory (Hilfiker et al., 2005), which might induce induce loss of SVs bound to the actin cytoskeleton.

On the other hand, the acceleration of SV cycling and the kinetics of SV fusion found in the PC-DCN synapses is opposite to that observed in the squid giant synapse. Although these observations strengthen a central role of domain E in the postdocking steps of neurotransmitter release, they reveal a more complex role of domain E in mammalian central inhibitory synapses. Thus, it is possible that pepE accelerates SV cycling within the RRP by interfering with the interactions of SV-associated synapsins with the actin-rich cytomatrix of the active and periactive zones (Bloom et al., 2003; Hilfiker et al., 2005), which, in mammalian synapses, might slow down SV cycling. This interpretation is supported by the observation that, in hippocampal nerve terminals, the disruption of the actin cytoskeleton resulted in both synapsin dispersion and faster SV cycling (Sankaranarayanan et al., 2003). However, the possibility that that peptide E interferes with a synapsin interactor that negatively regulates the rate of release cannot be excluded. Interestingly, the C-terminal region of synapsin has been reported to interact with Rab3A, a SV-associated GTPase regulating the final steps of release (Geppert et al., 1997; Giovedì et al., 2004a; Giovedì et al., 2004b; Schluter et al., 2006).

The phenotype of L7-pepE mice also confirms that the relative functional importance of the RP and RRP of SVs in sustaining release varies between neurons with different patterns of electrical activity. During short high-frequency trains that are likely to involve ‘kiss-and-run’ mechanisms and fast SV recycling pathways (Valtorta et al., 2001), mutant mice showed both a lower depression rate and a higher steady-state response than wild-type mice. Although the former effect might reflect lower release probability, this would imply no change in the steady-state level (Brenowitz and Trussell, 2001). The concomitant higher steady state observed suggests that the lower depression is due to an acceleration of SV cycling that allows faster refilling and slower depletion of the RRP.

It has been recently reported that mice lacking all synapsin isoforms have distinct deficits in excitatory and inhibitory synapses. Thus, glutamatergic terminals display normal release evoked by single stimuli and enhanced depression, whereas GABAergic terminals exhibit a decreased release in response to single stimuli and no effect on depression (Gitler et al., 2004b). Indeed, the recycling capacity of the RRP tends to be adapted to the activity pattern and is higher in terminals undergoing tonic high-frequency activity than in terminals experiencing infrequent phasic activation. Although the latter terminals take advantage of a large RP during bursting activity, the former have to rely on efficient recycling mechanisms (for reviews, see Brodin et al., 1997; Rizzoli and Betz, 2005). In vivo, PC neurons typically discharge at high frequencies (Thach, 1968; Thach, 1970; McDevitt et al., 1987). Thus, because of the very high basal firing rate, PCs are likely to rely predominantly on efficient recycling of the RRP rather than on SV recruitment from the RP. This is also suggested by the similar lower depression found in mutant mice during both short and sustained high-frequency trains, in the presence of a substantial depletion of the RP. Such RP depletion becomes apparent only under conditions of massive exocytosis that release SV from all nerve-terminal pools.

The data presented here demonstrate that overexpression of domain E increases synaptic strength at PC-DCN inhibitory synapses and participates in the motor behaviour phenotype observed in transgenic mice. These results might have important implications as to the role of synapsins in the regulation of central inhibitory synapses and network excitability. Synapsin knockout mice display a strong epileptic phenotype attributable to a specific deficit in inhibitory transmission (Terada et al., 1999; Gitler et al., 2004b). Moreover, the recently reported X-linked human epilepsy associated with a non-sense mutation of the SYN1 gene involves a truncation of the synapsin I C-terminal region that includes domain E (Garcia et al., 2004). It is tempting to speculate that the absence of this domain plays a crucial role in the impairment of synaptic inhibition leading to epileptiform activity.

Materials and Methods

Generation of L7-pepE mice

A minigene (*PepE*) was made by hybridization of two complementary oligonucleotides producing a double stranded product with 5′ overhangs compatible with BamHI restriction sites and coding for the last 25 residues of the rat synapsin Ia domain E. The sequences of the two oligonucleotides are as follows: PepE sense, 5′-GATCCGCCACCATGAGCCTGAGCCAGGACGAGGTGAAGG-CCGAGACCATCAGAAGCCTGAGAAAGAGCTTCGCCAGCCTGTTCAGCG-ACTAAG-3′; PepE antisense, 5′-ATCCTTAGTCGCTGAACAGGCTGGCGA-AGCTCTTTCTCAGGCTTCTGATGGTCTCGGCCTTCACCTCGTCCTGGCTC-AGGCTCATGGTGGCG-3′. The L7-pepE vector was constructed by inserting this fragment into the *Bam*HI site of pL7DAUG in which all the potential start codons were eliminated (De Zeeuw et al., 1998; Zhang et al., 2002). Thus, translation could only be initiated from the start codon provided within the inserted minigene, which was optimized with a Kozak sequence for efficient translation in mammalian cells (Kozak, 1986). The L7-PepE transgene, digested with *Hin*dIII/*Eco*RI, was injected into fertilized mouse eggs. Four positive transgenic lines were identified by PCR analysis and two of them (Tg-1 and Tg-2) were crossed to homozygosity. All animal procedures were approved by the Animal Care Committee of the University of Genova and by the Italian Ministry of Health.

RT-PCR analysis

RNA was extracted from brain tissue using TRI Reagent (Sigma). Reverse transcription was conducted with random examers and SuperScript II Reverse transcriptase (Invitrogen) as described previously (Corradi et al., 2003). Primers (forward, 5′-CAGGCCAGAACCCAGAAAG-3′; reverse, 5′-ATCCTTAGTCGC-TGAACAGG-3′) specific for the cDNA region encoding the L7-PepE were used for PCR amplification. Hypoxanthine guanine phosphoribosyltransferase (HPRT) primers used for normalization were 5′-TCCCTGGTTAAGCAGTACAG-3′ (forward) and 5′-GACGCAGCAACTGACATTTC-3′ (reverse).

In situ hybridization

Antisense oligonucleotides of 45 or 30 bases in length specific for the cDNA region encoding the L7-PepE were labelled at the 3′ end using [^{35}S]ATP (Amersham) and

terminal deoxynucleotidyl transferase (Roche). The hybridization of brain cryostat sections (14 μm thick) was carried out as previously described (Zoli et al., 1995). Briefly, sections were fixed with 4% paraformaldehyde (PFA), washed in 0.1M phosphate-buffered saline (PBS), acetylated and delipidated in ethanol and chloroform. After a 3 hour prehybridization in 0.6 M NaCl, 0.01 M dithiothreitol, 0.1 M Tris-HCl (pH 7.4), 0.05 M EDTA, 5% Denhardt's solution, 1 mg/ml Poly(A) (Roche), 10 mg/ml t-RNA, 1 mg/ml herring sperm DNA (Promega), 50% formamide at 37°C, sections were hybridized for 20 hours at 37°C with the labelled oligonucleotides. Sections were washed twice in 2× standard citrate solution (SSC, 3 M NaCl, 0.3 M sodium citrate) at room temperature, four times in 2× SSC at 54 or 48°C and twice in 1× SSC at room temperature. Sodium thiosulfate (63 mM) and β-mercaptoethanol (14.3 mM) were added to all washing solutions. After rinsing in ice-cold distilled water and drying, sections were first exposed to low-resolution autoradiographic film (Amersham) and then to high-resolution photographic emulsion (Kodak) for 1-2 months.

Immunohistochemistry

Mice were perfused under deep anesthesia (33 mg/kg xylazine and 33 mg/kg ketamine) with 0.1 M PBS followed by 4% paraformaldehyde (PFA) in 0.1 M PBS. After perfusion, brains were postfixed for 2 hours in 4% (w/v) PFA and transferred to 15% (w/v) sucrose in 0.1 M PBS and incubated overnight at 4°C. Cryostat sections (14 μm thick) were mounted on superfrost slides (Menzel-Glaser) and stored at –80°C for up to 15 days. Immunohistochemistry was performed as previously described (Fassio et al., 2000) using the following antibodies: monoclonal anti-calbindin D-28K (Sigma), anti-VAMP2 (Synaptic Systems), polyclonal anti-synaptophysin (G111), anti-synapsin I (G177) and anti-synapsin pepE (G304) raised in our laboratory (Valtorta et al., 1988; Pieribone et al., 1995; Vaccaro et al., 1997). Primary antibodies were detected using either the avidin-biotin method with diaminobenzidine as a chromogen (Vector Laboratories) or Alexa Fluor 488- and 546-conjugated secondary antibodies (Invitrogen). Specimens were viewed with an epifluorescence Olympus inverted microscope. Images were recorded with a Hamamatsu C4742-98 ORCA II camera and processed using Image Pro Plus 4.5 (Media Cybernetics). DCN sections, double-labeled with anti-calbindin and anti-synaptophysin antibodies, were subjected to confocal scanning microscopy (Biorad MRC1024). Stacks of images were acquired in the DCN region at 1.5 μm intervals along the *z*-axis. Based on synaptophysin staining, synaptic masks were generated by using the granulometric algorithm (Prodanova et al., 2006). The synaptic signal of calbindin was obtained by applying the synaptic mask to the calbindin signal. Nerve terminal counts were performed by using the 'analyze particle' function of the Image J program (NIH, Bethesda, MD).

Primary cultures

Primary cultures of PC were prepared from E18 Tg-2 mice following the reported procedure (Tabata et al., 2000). Cultures were either subjected to immunocytochemistry with anti-calbindin and anti-pepE antibodies or harvested, solubilized in stop solution and subjected to SDS-PAGE in Tris-Tricine (Schagger and von Jagow, 1987) and immunoblotting of PVDF membranes with anti-pepE antibodies.

Primary hippocampal neurons obtained from E18 wild-type embryos (Banker and Cowan, 1977) were transfected at 5 days in vitro (DIV) with either pEGFP, pEGFP-synapsin Ia or pEGFP-domain E vector using Effectene (Qiagen). Expression and targeting of GFP or of the GFP chimeras were followed at 7-9 DIV by fluorescence microscopy of neurons labelled with anti-VAMP2 antibodies.

Behavioral analysis

Mice (3 months old, weighing 20-25 g) housed under standard temperature, humidity and light/dark cycle underwent the following tests during the light phase:

Horizontal bar test

The mouse was placed on a round (2 cm diameter, 50 cm length) rod 35 cm elevated from the bench. The latency to fall was measured in three separate trials (with a 5 minute intertrial interval). Each trial ended at 180 seconds.

Vertical pole test

The mouse was placed facing up on a pole (2 cm diameter, 50 cm long). The end of the pole was then gradually lifted to a vertical position and the time the mouse stayed on the pole was recorded for a maximum of 60 seconds. Time values were converted to a pole test score as follows: stayed on 60 seconds and climbed halfway down the pole=8; climbed to the lower half of the pole=9; climbed down and got off the pole in 51-60 seconds=10, 41-50 seconds=11, 31-40 seconds=12, 21-30 seconds=13, 11-20 seconds=14, 1-10 seconds=15 (McIlwain et al., 2001). Scores lower than 8 refer to animals that fall from the pole, an event that never occurred with transgenic animals. Each animal was tested in three consecutive trials.

Rota-rod test

Mice were tested with the rota-rod (Ugo Basile, Via G. Borghi 43, 20125 Comerio, VA, Italy) under conditions of either constant speed or constant acceleration (Nolan et al., 2003). In the constant-speed test, mice were first trained until they could remain on the rod at 4 rpm for three consecutive 120-second trials. The next day the mice were placed back on the rod for a trial at 40 rpm. The time a mouse could remain on the rota rod (maximum 120 seconds) was recorded and the process was repeated for speeds of 30, 20 and 4 rpm. Animals were given four trials per day with a 1-hour inter-trial interval. In the accelerating test, mice were placed on the rota rod starting at 4 rpm, slowly accelerating to 40 rpm. The maximum observation time was 5 minutes. Animals were tested for 3 consecutive days, receiving four trials on day 1 and three trials on both days 2 and 3, with a 1-hour inter-trial interval.

Gait analysis

Mice were put in a dark tunnel (7 cm wide, 50 cm long, 10 cm high) with white paper on the floor. Before traversing the tunnel, the hindpaws of the animals were dipped in non-toxic black ink (Feil et al., 2003). Footprints were analyzed using the 'Footprint 1.22' software (Klapdor et al., 1997) to calculate stride width, stride length and maximum difference in stride-length values.

[^{3}H]GABA release from DCN synaptosomes

Mice were killed by decapitation and DCN were rapidly dissected out. Percoll-purified synaptosomes were prepared as previously described (Dunkley et al., 1988). Synaptosomes were resuspended in physiological medium with the following composition (mM): NaCl 125, KCl 3, $MgSO_4$ 1.2, $CaCl_2$ 1.2, NaH_2PO_4 1, $NaHCO_3$ 22, glucose 10 (pH 7.4 when equilibrated with 95% O_2 and 5% CO_2); and incubated at 37°C for 15 minutes in the presence of 0.04 μM [^{3}H]GABA. After labelling, aliquots of the suspensions (<100 μg protein/filter) were stratified onto microporous filters at the bottom of parallel superfusion chambers maintained at 37°C (Raiteri and Raiteri, 2000) and superfused with standard medium at 0.5 ml/minute. Under these conditions, synaptosomes constitute less than a monolayer and indirect effects mediated by compounds released by neighbouring particles are virtually absent. After a 33-minute equilibration period, four 3-minute fractions were collected. Synaptosomes were exposed to a 90-second pulse of high KCl (12, 15 or 35 mM) or ionomycin (0.5 mM) at the end of the first fraction collected (*t*=39 minutes). In some experiments, three successive high-KCl pulses were applied to the same synaptosomal preparation at 18-minute intervals (*t*=39, 57 and 75 minutes). Aminooxyacetic acid (50 μM) was present throughout the experiment to prevent [^{3}H]-GABA metabolism. Collected samples and filters were counted for radioactivity. The amount of radioactivity present in each sample was calculated as fractional rate and the stimulus-evoked overflow was estimated by subtracting basal release from the radioactivity measured in the samples collected during and after the stimulation pulse.

Electrophysiological recordings in cerebellar slices

Whole-cell patch-clamp recordings from cerebellar slices were performed following standard procedures (D'Angelo et al., 1995; Hansel et al., 2001; Sola et al., 2004). Parasagittal slices (220 μm thick) were taken from the cerebellar vermis of P8-P12 mice decapitated after deep halothane anesthesia. During the slicing procedure, the cerebellar vermis was immersed in a cold solution containing (mM): K-gluconate 130, KCl 15, EGTA 0.2, HEPES 20, Glucose 10 (pH 7.4 with NaOH). Before recording, slices were incubated at 32°C for at least 30 minutes in oxygenated bicarbonate-buffered saline (standard Krebs solution) containing (mM): NaCl 120, KCl 2, $MgSO_4$ 1.2, $NaHCO_3$ 26, KH_2PO_4 1.2, $CaCl_2$ 2, glucose 11 (pH 7.4 when equilibrated with 95% O_2 and 5% CO_2). Slices were then transferred into the recording chamber and perfused at 1.5 ml/minute with oxygenated Krebs solution at room temperature (20-23°C). The Krebs solution was added with 50 mM D-APV (D-2-amino-5-phosphonovaleric acid) and 20 mM CNQX (6-cyano-7-nitroquinoxaline-2,3-dione) (Tocris). Slices were visualized with an upright epifluorescence microscope (Zeiss Axioskop 2FS), equipped with a ×63 water-immersion objective (0.9 NA) and DIC optics, using infrared illumination (illumination filter 750 nm) and an IR CCD camera (T.I.L.L. Photonics). Recordings were obtained using a MultiClamp 700A amplifier (Molecular Devices).

Whole-cell recordings were performed from large spheroidal neurons (maximum diameter 15-30 μm) identified with DIC-IR Nomarsky interference contrast. These neurons showed spontaneous firing at >10 Hz in cell-attached before obtaining the whole-cell configuration. The input resistance measured by recording the response to –10 mV voltage steps delivered from the holding potential of –65 mV was 440.9 54.1 MΩ (*n*=10). Thus, these neurons corresponded to type-I DCN projection neurons according to the previously reported classification (Czubayko et al., 2001) (see also Anchisi et al., 2001). The patch-pipette contained (mM): Cs_2SO_4 81, NaCl 4, $MgSO_4$ 2, $CaCl_2$ 0.02, BAPTA 0.1, glucose 15, ATP-Mg 3, GTP 0.1, HEPES 15, QX314 1.5. This solution maintained resting free [Ca^{2+}] at 100 nM and pH was adjusted to 7.2 with CsOH. Patch-clamp pipettes filled with this solution had a resistance of 1-2 MΩ before seal formation. After obtaining the whole-cell configuration, membrane potential of DCN neurons was kept at –65 mV. PC axons were stimulated via a stimulus isolation unit with a bipolar silver wire, whose active filament was inserted into a glass pipette (10 μm tip diameter) filled with standard Krebs solution. The stimulating electrode was placed at 100 20 μm from the recorded DCN neuron. IPSCs were elicited at a basal frequency of 0.1 Hz with constant stimulation intensity. Two types of high-frequency trains were applied: (1) 200 milliseconds at 100 Hz to analyze short-term plasticity regulated by RRP and

(2) 120 seconds at 50 Hz to investigate the involvement of the RP. IPSC peak value was calculated as the difference between peak and base (see Fig. 5). Under the same conditions, PC spike firing was monitored using loose cell-attached recordings that do not perturb basal discharge frequency (Forti et al., 2006).

Electron microscopy

Chopper sections containing DCN from three wild-type and three Tg-2 mice were fixed for 30 minutes at room temperature with 2% PFA, 1% glutaraldehyde, 1% sucrose in cacodylate buffer (100 mM, pH 7.4), washed five times in cacodylate buffer, and postfixed for 1 hour with 1% OsO_4 in the same buffer. Samples were subsequently washed five times for 5 minutes with cacodylate buffer, dehydrated and embedded in Epon 812 (Ceccarelli et al., 1973). Silver-gray sections were cut on a microtome (Reichert-Jung Ultracut), stained with 4% uranyl acetate, 0.4% lead citrate, and examined in a Hitachi H-7000 electron microscope. The identification of the PC-DCN synapses was carried out based on the following criteria: (1) Gray type II 'symmetrical' synapses; (2) elliptical and dispersed SVs; (3) location on soma or proximal dendrites of DCN neurons (Chan-Palay, 1977). All the encountered synapses whose features made them recognizable as PC nerve endings were analyzed. The geometrical parameters of the nerve endings as well as the SV density measured in samples from wild-type mice were virtually identical to those reported (Chan-Palay, 1977), indicating that the sample was representative of the whole population of PC nerve endings.

Morphometric analysis

Digitized electron micrographs of PC-DCN synapses were subjected to computer-assisted morphometric analysis to calculate the following parameters: nerve terminal area, length of the synaptic contact, number and length of active zone, number of SVs and, for each SV, the distance from the closest active zone and the mean distance from all surrounding SVs (mean intervesicular distance, MID, a measure of SV clustering). Since MID depends on SV density, a clustering index was obtained, corresponding to the ratio between the MID calculated for a simulated homogeneous SV distribution and the measured MID. The area occupied by mitochondria (which was similar in the two experimental groups) was subtracted from the total area. Parameters were calculated from the EM images of 60 synapses from three wild-type mice and 54 synapses from three transgenic mice. Within each animal, individual PC-DCN synapses were analyzed to give mean individual values that were subsequently averaged within the same experimental group. To analyze SV distribution with respect to the active zone, the calculated distances of SVs from active zone within each nerve terminal were grouped into 50 classes of 50 nm. From the frequency of SVs whose distance from the active zone was falling in the various classes, frequency distribution histograms were obtained for each nerve terminal and were subsequently averaged within the same experimental group.

Statistical analysis

Data are reported as mean ± s.e.m. and statistical analysis was performed using the program Prism (GraphPad Software). Data were analyzed using one-way ANOVA followed by either the Student's *t*-test or multiple comparison tests (either Dunnett, Duncan or Newman-Kleus test). Frequency distribution histograms were analyzed by the Kolmogorov-Smirnov normality test followed by either parametric or non-parametric tests (Student's *t*-test and Mann-Whitney *U* test, respectively). Both types of analysis gave fully comparable significance levels.

We thank P. Greengard (The Rockefeller University, New York, NY) for useful discussion and critical reading of the manuscript, L. Pozzi and C. Tiveron (Telethon Transgenic Mice Service Center, Istituto Regina Elena, Roma, Italy) for embryo injections, M. Zoli and A. Zanardi (University of Modena, Italy) for help with in situ hybridization experiments, D. Ghezzi (Politecnico di Milano, Italy) for help with the morphometric analysis. This work was supported by grants from the Italian Ministry of University (Cofin 2004 and 2005, FIRB 'Neuroscienze' and 'Postgenomica' to F.B., G.B., E.D'A. and F.V.), Fisher Foundation for Alzheimer's Disease Research, Associazione Italiana Ricerca sul Cancro, Fondazione Franco e Luisa Mariani and Consorzio Italiano Biotecnologie (to F.B.), Consiglio Nazionale delle Ricerche (Progetti Strategici Neuroscienze and Genomica Funzionale to F.B. and F.V.) and by projects of the European Community (Cerebellum QLG3-CT-2001-02256 and Spikeforce IST-2001035271 to E.D'A). The financial support of Telethon-Italy (grant no. GGP05134 to F.B and F.V.) is gratefully acknowledged.

References

Aizenman, C. D., Manis, P. B. and Linden, D. J. (1998). Polarity of long-term synaptic gain change is related to postsynaptic spike firing at a cerebellar inhibitory synapse. *Neuron* **21**, 827-835.

Anchisi, D., Scelfo, B. and Tempia, F. (2001). Postsynaptic currents in deep cerebellar nuclei. *J. Neurophysiol.* **85**, 323-331.

Ashton, A. C. and Dolly, J. O. (2000). A late phase of exocytosis from synaptosomes induced by elevated $[Ca^{2+}]_i$ is not blocked by clostridial neurotoxins. *J. Neurochem.* **74**, 1979-1988.

Banker, G. A. and Cowan, W. M. (1977). Rat hippocampal neurons in dispersed cell culture. *Brain Res.* **126**, 397-342.

Benfenati, F., Valtorta, F., Chieregatti, E. and Greengard, P. (1992a). Interaction of free and synaptic vesicle-bound synapsin I with F-actin. *Neuron* **8**, 377-386.

Benfenati, F., Valtorta, F., Rubenstein, J. L., Gorelick, F. S., Greengard, P. and Czernik, A. J. (1992b). Synaptic vesicle-associated Ca^{2+}/calmodulin-dependent protein kinase II is a binding protein for synapsin I. *Nature* **359**, 417-420.

Bloom, O., Evergren, E., Tomilin, N., Kjaerulff, O., Low, P., Brodin, L., Pieribone, V. A., Greengard, P. and Shupliakov, O. (2003). Colocalization of synapsin and actin during synaptic vesicle recycling. *J. Cell Biol.* **161**, 737-747.

Bonanomi, D., Menegon, A., Miccio, A., Ferrari, G., Corradi, A., Kao, H. T., Benfenati, F. and Valtorta, F. (2005). Phosphorylation of synapsin I by cAMP-dependent protein kinase controls synaptic vesicle dynamics in developing neurons. *J. Neurosci.* **25**, 7299-7308.

Brenowitz, S. and Trussell, L. O. (2001). Maturation of synaptic transmission at end-bulb synapses of the cochlear nucleus. *J. Neurosci.* **21**, 9487-9498.

Brodin, L., Low, P., Gad, H., Gustaffson, J., Pieribone, V. A. and Shupliakov, O. (1997). Sustained neurotransmitter release: new molecular clues. *Eur. J. Neurosci.* **9**, 2503-2511.

Ceccaldi, P., Grohovaz, F., Benfenati, F., Chieregatti, E., Greengard, P. and Valtorta, F. (1995). Dephosphorylated synapsin I anchors synaptic vesicles to actin cytoskeleton: an analysis by videomicroscopy. *J. Cell Biol.* **128**, 905-912.

Ceccarelli, B., Hurlbut, W. P. and Mauro, A. (1973). Turnover of transmitter and synaptic vesicles at the frog neuromuscular junction. *J. Cell Biol.* **57**, 499-524.

Chan-Palay, V. (1977). *Cerebellar Dentate Nucleus*. Berlin: Springer Verlag.

Chi, P., Greengard, P. and Ryan, T. A. (2001). Synapsin dispersion and reclustering during synaptic activity. *Nat. Neurosci.* **4**, 1187-1193.

Chi, P., Greengard, P. and Ryan, T. A. (2003). Synaptic vesicle mobilization is regulated by distinct synapsin I phosphorylation pathways at different frequencies. *Neuron* **10**, 69-78.

Clark B. A., Mansivois P., Branco T., London M. and Hausser M. (2005). The site of action potential initiation in cerebellar Purkinje neurons. *Nat. Neurosci.* **8**, 137-139.

Corradi, A., Croci, L., Broccoli, V., Zecchini, S., Previtali, S., Wurst, W., Amadio, S., Maggi, R., Quattrini, A. and Consalez, G. G. (2003). Hypogonadotropic hypogonadism and peripheral neuropathy in Ebf2-null mice. *Development* **130**, 401-410.

Czubayko, U., Sultan, F., Thier, P. and Schwarz, C. (2001). Two types of neurons in the rat cerebellar nuclei as distinguished by membrane potentials and intracellular fillings. *J. Neurophysiol.* **85**, 2017-2029.

D'Angelo, E., De Filippi, G., Rossi, P. and Taglietti, V. (1995). Synaptic excitation of individual rat cerebellar granule cells in situ: evidence for the role of NMDA receptors. *J. Physiol. Lond.* **484**, 397-413.

De Zeeuw, C. I., Hansel, C., Bian, F., Koekkoek, S. K. E., van Alphen, A. M., Linden, D. J. and Oberdick, J. (1998). Expression of a protein kinase C inhibitor in Purkinje cells blocks cerebellar LTD and adaptation of the vestibulo-ocular reflex. *Neuron* **20**, 495-508.

Dunkley, P. R., Heath, J. W., Harrison, S. M., Jarvie, P. E., Glenfield, P. J. and Rostas, J. A. (1988). A rapid Percoll gradient procedure for isolation of synaptosomes directly from an S1 fraction homogeneity and morphology of subcellular fractions. *Brain Res.* **441**, 59-71.

Fassio, A., Evans, G., Grisshammer, R., Bolam, J. P., Mimmack, M. and Emson, P. C. (2000). Distribution of neurotensin receptor NTS1 in the rat CNS studied using an amino-terminal directed antibody. *Neuropharmacology* **39**, 1430-1442.

Feil, R., Hartmann, J., Luo, C., Wolfsgruber, W., Schilling, K., Feil, S., Barski, J. J., Meyer, M., Konnerth, A., De Zeeuw, C. I. et al. (2003). Impairment of LTD and cerebellar learning by Purkinje cell-specific ablation of cGMP-dependent protein kinase I. *J. Cell Biol.* **163**, 295-302.

Forti, L., Cesana, E., Mapelli, J. and D'Angelo, E. (2006). Ionic mechanisms of autorhythmic firing in cerebellar Golgi cells. *J. Physiol.* **574**, 711-729.

Garcia, C. C., Blair, H. J., Seager, M., Coulthard, A., Tennant, S., Buddles, M., Curtis, A. and Goodship, J. A. (2004). Identification of a mutation in synapsin I, a synaptic vesicle protein, in a family with epilepsy. *J. Med. Genet.* **41**, 183-186.

Geppert, M., Goda, Y., Stevens, C. F. and Südhof, T. C. (1997). The small GTP-binding protein Rab3A regulates a late step in synaptic vesicle fusion. *Nature* **387**, 810-814.

Giovedì, S., Vaccaro, P., Valtorta, F., Darchen, F., Greengard, P., Cesareni, G. and Benfenati, F. (2004a). Synapsin is a novel Rab3 effector protein on small synaptic vesicles. I. Identification and characterization of the synapsin I-Rab3 interactions in vitro and in intact nerve terminals. *J. Biol. Chem.* **279**, 43760-43768.

Giovedì, S., Darchen, F., Valtorta, F., Greengard, P. and Benfenati, F. (2004b). Synapsin is a novel Rab3 effector protein on small synaptic vesicles. II. Functional effects of the Rab3A-synapsin I interaction. *J. Biol. Chem.* **279**, 43769-43779.

Gitler, D., Xu, Y., Kao, H. T., Lin, D., Lim, S., Feng, J., Greengard, P. and Augustine, G. J. (2004a). Molecular determinants of synapsin targeting to presynaptic terminals. *J. Neurosci.* **24**, 3711-3720.

Gitler, D., Takagishi, Y., Feng, J., Ren, Y., Rodriguiz, R., Wetsel, W. C., Greengard, P. and Augustine, G. J. (2004b). Different presynaptic roles of synapsins at excitatory and inhibitory synapses. *J. Neurosci.* **24**, 11368-11380.

Greengard, P., Valtorta, F., Czernik, A. J. and Benfenati, F. (1993). Synaptic vesicle phosphoproteins and regulation of synaptic function. *Science* **259**, 780-785.
Hansel, C., Linden, D. J. and D'Angelo, E. (2001). Beyond parallel fiber LTD: the diversity of synaptic and non-synaptic plasticity in the cerebellum. *Nat. Neurosci*. **4**, 467-475.
Hilfiker, S., Schweizer, F. E., Kao, H. T., Czernik, A. J., Greengard, P. and Augustine, G. J. (1998). Two sites of action for synapsin domain E in regulating neurotransmitter release. *Nat. Neurosci*. **1**, 29-35.
Hilfiker, S., Pieribone, V. A., Czernik, A. J., Kao, H. T., Augustine, G. J. and Greengard, P. (1999). Synapsins as regulators of neurotransmitter release. *Philos. Trans. R. Soc. Lond. B Biol. Sci.* **354**, 269-279.
Hilfiker, S., Benfenati, F., Doussau, F., Nairn, A. C., Czernik, A. J., Augustine, G. J. and Greengard, P. (2005). Structural domains involved in the regulation of transmitter release by synapsins. *J. Neurosci.* **25**, 2658-2669.
Hosaka, M., Hammer, R. E. and Südhof, T. C. (1999). A phospho-switch controls the dynamic association of synapsins with synaptic vesicles. *Neuron* **24**, 377-387.
Humeau, Y., Dousseau, F., Vitiello, F., Greengard, P., Benfenati, F. and Poulain, B. (2001). Synapsin controls transition between multiple synaptic vesicle stores during short-term plasticity. *J. Neurosci.* **21**, 4195-4206.
Jovanovic, J. N., Benfenati, F., Siow, Y. L., Sihra, T. S., Sanghera, J. S., Pelech, S. L., Greengard, P. and Czernik, A. J. (1996). Neurotrophins stimulate phosphorylation of synapsin I by MAP kinase and regulate synapsin I-actin interactions. *Proc. Natl. Acad. Sci. USA* **93**, 3679-3683.
Kao, H. T., Porton, B., Hilfiker, S., Stefani, G., Pieribone, V. A., DeSalle, R. and Greengard, P. (1999). Molecular evolution of the synapsin gene family. *J. Exp. Zool.* **285**, 360-377.
Klapdor, K., Dulfer, B. G., Hammann, A. and Van der Staay, F. J. (1997). A low cost method to analyze footprint patterns. *J. Neurosci. Methods* **75**, 49-54.
Kozak, M. (1986). Pont mutation define a sequence flanking the AUG initiator codon that modulates translation by eukaryotic ribosomes. *Cell* **47**, 481-483.
Li, L., Chin, L. S., Shupliakov, O., Brodin, L., Sihra, T. S., Hvalby, O., Jensen, V., Zheng, D., McNamara, J. O., Greengard, P. et al. (1995). Impairment of synaptic vesicle clustering and of synaptic transmission, and increased seizure propensity, in synapsin I-knockout mice. *Proc. Natl. Acad. Sci. USA* **92**, 9235-9239.
McDevitt, C. J., Ebner, T. J. and Bloedel, J. R. (1987). Changes in the responses of cerebellar nuclear neurons associated with the climbing fiber response of Purkinje cells. *Brain Res*. **425**, 14-24.
McIlwain, K. L., Merriweather, M. Y., Yuva-Paylor, L. A. and Paylor, R. (2001). The use of behavioral test batteries: effects of training history. *Physiol. Behav*. **73**, 705-717.
Morishita, W. and Sastry, B. R. (1996). Postsynaptic mechanisms underlying long-term depression of GABAergic transmission in neurons of the deep cerebellar nuclei. *J. Neurophysiol*. **76**, 59-68.
Nolan, M. F., Malleret, G., Lee, K. H., Gibbs, E., Dudman, J. T., Santoro, B., Yin, D., Thompson, R. F., Siegelbaum, S. A., Kandel, E. R. et al. (2003). The hyperpolarization-activated HCN1 channel is important for motor learning and neuronal integration by cerebellar Purkinje cells. *Cell* **115**, 551-564.
Ouardouz, M. and Sastry, B. R. (2000). Mechanisms underlying LTP of inhibitory synaptic transmission in the deep cerebellar nuclei. *J. Neurophysiol*. **84**, 1414-1421.
Pedroarena, C. M. and Schwarz, C. (2003). Efficacy and short-term plasticity at GABAergic synapses between Purkinje and cerebellar nuclei neurons. *J. Neurophysiol*. **89**, 704-715.
Pieribone, V. A., Shupliakov, O., Brodin, L., Hilfiker-Rothenfluh, S., Czernik, A. J. and Greengard, P. (1995). Distinct pools of synaptic vesicles in neurotransmitter release. *Nature* **37**, 493-497.
Porton, B., Kao, H. T. and Greengard, P. (1999). Characterization of transcripts from the synapsin III locus. *J. Neurochem*. **73**, 2266-2271.
Prodanova, D., Heeromac, J. and Marania, E. (2006). Automatic morphometry of synaptic boutons of cultured cells using granulometric analysis of digital images. *J. Neurosci. Methods* **151**, 168-177.
Raiteri, L. and Raiteri, M. (2000). Synaptosomes still viable after 25 years of superfusion. *Neurochem. Res*. **25**, 1265-1274.
Rizzoli, S. O. and Betz, W. J. (2005). Synaptic vesicle pools. *Nat. Rev. Neurosci*. **6**, 57-69.
Rosahl, T. W., Spillane, D., Missler, M., Herz, J., Selig, D. K., Wolff, J. R., Hammer, R. E., Malenka, R. C. and Südhof, T. C. (1995). Essential functions of synapsins I and II in synaptic vesicle regulation. *Nature* **375**, 488-493.
Sankaranarayanan, S., Atluri, P. P. and Ryan, T. A. (2003). Actin has a molecular scaffolding, not propulsive, role in presynaptic function. *Nat. Neurosci*. **6**, 127-135.
Schagger, H. and von Jagow, G. (1987). Tricine-sodium dodecyl sulfate-polyacrylamide gel electrophoresis for the separation of proteins in the range from 1 to 100 kDa. *Anal. Biochem*. **166**, 368-379.
Schluter, O. M., Basu, J., Südhof, T. C. and Rosenmund, C. (2006). Rab3 superprimes synaptic vesicles for release: implications for short-term synaptic plasticity. *J. Neurosci*. **26**, 1239-1246.
Sola, E., Prestori, F., Rossi, P., Taglietti, V. and D'Angelo, E. (2004). Increased neurotransmitter release during long-term potentiation at mossy fibre-granule cell synapses in rat cerebellum. *J. Physiol*. **557**, 843-861.
Stigliani, S., Raiteri, L., Fassio, A. and Bonanno, G. (2003). The sensitivity of catecholamine release to botulinum toxin C1 and E suggest selective targeting of vesicles set into the readily releasable pool. *J. Neurochem*. **85**, 409-421.
Südhof, T. C., Czernik, A. J., Kao, H. T., Takei, K., Johnston, P. A., Horiuchi, A., Kanazir, S. D., Wagner, M. A., Perin, M. S., De Camilli, P. et al. (1989). Synapins: mosaic of shared and individual domains in a family of synaptic vesicle phosphoproteins. *Science* **245**, 1474-1480.
Tabata, T., Sawada, S., Araki, K., Bono, Y., Furuya, S. and Kano, M. (2000). A reliable method for culture of dissociated mouse cerebellar cells enriched for Purkinje neurons. *J. Neurosci. Methods* **104**, 45-53.
Telgkamp, P. and Raman, I. M. (2002). Depression of inhibitory synaptic transmission between Purkinje cells and neurons of the cerebellar nuclei. *J. Neurosci*. **22**, 8447-8457.
Telgkamp, P., Padgett, D. E., Ledoux, V. A., Woolley, C. S. and Raman, I. M. (2004). Maintenance of high-frequency transmission at Purkinje to cerebellar nuclear synapses by spillover from boutons with multiple release sites. *Neuron* **41**, 113-126.
Terada, S., Tsujimoto, T., Takei, Y., Takahashi, T. and Hirokawa, N. (1999). Impairment of inhibitory synaptic transmission in mice lacking synapsin I. *J. Cell Biol*. **145**, 1039-1048.
Thach, W. T. (1968). Discharge of Purkinje and cerebellar nuclear neurons during rapidly alternating arm movements in the monkey. *J. Neurophysiol*. **31**, 785-797.
Thach, W. T. (1970). Discharge of cerebellar neurons related to two maintained postures and two prompt movements. II. Purkinje cell output and input. *J. Neurophysiol*. **33**, 527-536.
Vaccaro, P., Dente, L., Onofri, F., Zucconi, A., Martinelli, S., Valtorta, F., Greengard, P., Cesareni, G. and Benfenati, F. (1997). Epitope mapping on mammalian synapsins using phage display libraries. *Mol. Brain Res*. **52**, 1-16.
Valtorta, F., Villa, A., Jahn, R., De Camilli, P., Greengard, P. and Ceccarelli, B. (1988). Localization of synapsin I at the frog neuromuscular junction. *Neuroscience* **24**, 593-603.
Valtorta, F., Meldolesi, J. and Fesce, R. (2001). Synaptic vesicles: is kissing a matter of competence? *Trends Cell Biol*. **11**, 324-328.
Zhang, X., Zhang, H. and Oberdick, J. (2002). Conservation of the developmentally regulated dendritic localization of a Purkinje cell-specific mRNA that encodes a G-protein modulator: comparison of rodent and human Pcp2(L7) gene structure and expression. *Brain Res. Mol. Brain Res*. **105**, 1-10.
Zoli, M., Le Novere, N., Hill, J. A. and Changeux, J. P. (1995). Developmental regulation of nicotinic ACh receptor subunit mRNAs in the rat central and peripheral nervous systems. *J. Neurosci*. **15**, 1912-1939.